ACS OMEGA

http://pubs.acs.org/journal/acsodf

Article

Selective and Sensitive Electrochemical Sensor for Aflatoxin M1 with a Molybdenum Disulfide Quantum Dot/Metal−Organic Framework Nanocomposite

Gurjeet Kaur, Saloni Sharma, Shalini Singh, Neha Bhardwaj, and Akash Deep*

Cite This: *ACS Omega* 2022, 7, 17600−17608

Read Online

ACCESS | Metrics & More | Article Recommendations

ABSTRACT: Aflatoxins are the hepatotoxic secondary metabolites which are highly carcinogenic and known to cause several adverse effects on human health. The present study reports a simple, sensitive, and novel electrochemical sensor for aflatoxin M1 (AFM1). The sensor has been fabricated by modifying the screen-printed carbon electrodes with a functional nanocomposite of molybdenum disulfide (MoS_2) quantum dots (QDs) and a zirconium-based metal−organic framework (MOF), that is, UiO-66-NH_2. The MoS_2/UiO-66-modified electrodes were decorated with the AFM1-specific monoclonal antibodies and then investigated for the electrochemical detection of AFM1. Based on the electrochemical impedance spectroscopy analysis, it was possible to detect AFM1 in the concentration range of 0.2−10 ng mL^{-1} with a limit of detection of 0.06 ng mL^{-1}. The realization of an excellent sensing performance can be attributed to the electroactivity of MoS_2 QDs and the large surface to volume area achieved by the addition of the MOF. The presence of UiO-66-NH_2 is also useful to attain readily available amine functionality for the robust interfacing of antibodies. The performance of the developed sensor has also been validated by detecting AFM1 in the spiked milk samples.

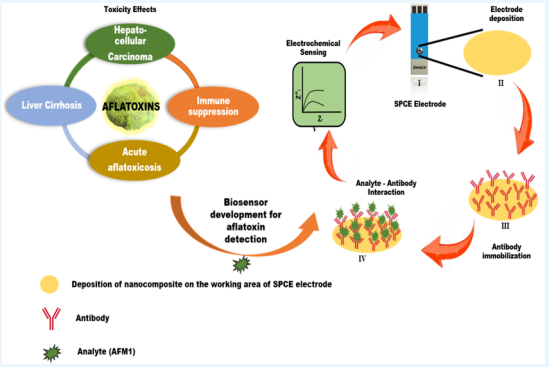

1. INTRODUCTION

Aflatoxins (AFs) are mycotoxins produced as the highly toxic metabolites by different fungi, such as *Fusarium*, *Aspergillus*, and *Penicillium*. AFs particularly AFB1, AFB2, and AFG1 are known to be carcinogenic, mutagenic, and teratogenic. They are known to inflict several health risks in humans.[1] AF M1 (AFM1) is the hydroxylated form of AFB1. It is mainly secreted in the milk of mammals that consume AFB1-contaminated feed.[2] The consumption of the AFM1-contaminated food (e.g., milk and dairy products) can lead to severe health problems including decreased immune response, reduced functioning of the liver, and increased susceptibility to infections.[3] AFM1 has been qualified as a group I carcinogen by the International Agency for Research on Cancer. Due to its hepatotoxicity and potential carcinogenicity, different regulatory agencies have regulated maximum permissible levels for AFM1 in milk, ranging from 0.025 to 0.5 $\mu g\ L^{-1}$.[4] Therefore, the monitoring of AFM1 in food has become essential to protect consumers from its dangers and ensure the safety of the food products.

Conventional methods, such as thin-layer chromatography, high-performance liquid chromatography (HPLC)-fluorescent detection, liquid chromatography−tandem mass spectrometry (LC−MS/MS), and LC/atmospheric pressure chemical ionization MS, have been commonly used for the detection of AFM1.[5] In addition to these, immunoassays such as enzyme-linked immunosorbent assay have also been developed.[6] Nevertheless, the biosensors for AF bear a special significance as they can satisfy the demands of rapid, cost-effective, point-of-care, portable, and sensitive analytical systems for AFM1. The use of nanomaterials in the development of biosensors has gained tremendous importance.[7] As potential food safety monitoring tools, the electrochemical sensors are projected as valuable tools to determine various biological/ecological parameters as well as monitor diverse inorganic and organic pollutants. Due to the features of fast detection rates, low cost, high sensitivity, and easy adaptability, the electrochemical sensors have also gained considerable attention for the quantitative detection of AF.[8] In recent years, most of such developments were based on the use of nanomaterials and their composites, such as ZnS quantum dots (QDs), AuNP/CuCoPBA, NH_2−Co-MOF, and so forth.[9] The use of nanomaterials in electrochemical detection

Received: January 7, 2022
Accepted: April 27, 2022
Published: May 19, 2022

platforms offers high conductivity and strong binding interactions with the receptors. The above-mentioned sensors have been reported with quick response time, simplicity, high specificity, and better portability to facilitate the detection of AF. The common transducer mechanisms used in the conventional electrochemical sensors follow amperometric, voltametric, impedimetric, potentiometric, and conductometric approaches.

Among the different advanced functional materials being explored for the development of electrochemical biosensors, molybdenum disulfide (MoS_2) and metal−organic frameworks (MOFs) have established their unique reputations.[10] The nanoforms of MoS_2 offer the advantages of both direct and indirect band gap properties, and they have been advocated highly useful in electrochemical and optical sensors.[11] In particular, the MoS_2 QDs are easier to synthesize with better control on the shape and morphology.[11b,c,12] Their addition to other matrices like MOFs can deliver the realization of interesting composite films with fascinating chemical and physical properties, for example, a high surface area, desirable film conductivity due to the filler effect, and readily available functionality for required bioconjugations.[13] Such composite thin films can be explored for the development of novel electrochemical sensors.[14]

The present research work, for the first time, explores the use of a MoS_2/MOF composite for the development of an electrochemical biosensor for the detection of AFM1. Due to many desirable platform properties, as listed above, we have been able to realize an outstanding sensor performance delivering the quantification of AFM1 over a wide concentration range and with a low limit of detection (LOD). The sensor has also worked excellently for the analysis of spiked milk samples.

2. EXPERIMENTAL SECTION

2.1. Materials and Characterization Tools. AFM1 and its monoclonal antibody were purchased from Sigma-Aldrich, India, and Abcam, India, respectively. Zirconium chloride ($ZrCl_4$), 2-aminoterephthalic acid (NH_2BDC), ferric chloride hexahydrate ($FeCl_3{\cdot}6H_2O$), ammonium molybdate tetrahydrate, L-cysteine, and other solvents were also purchased from Sigma, India. The screen-printed carbon electrodes (SPCEs) were purchased from Zensor, Taiwan.

The morphological studies were carried out using a field emission scanning electron microscope system (Hitachi SU8010, Japan). The spectroscopic and structural characterizations were carried out using a UV−vis spectrophotometer (Varian Cary 5000), a Fourier-transform infrared spectrometer (Nicolet iS10, USA), and an X-ray diffractometer (D8 Advanced, Bruker, Germany, Kα = 1.54 Å). MoS_2 QDs were synthesized via the microwave route with the aid of a dedicated microwave synthesizer reactor from Anton Paar (Monowave 200). The electrochemical investigations were carried out using an electrochemical analyzer (CHI 660 C, USA, current measurement resolution: <0.01 pA). These experiments were performed in a phosphate buffer medium (PBS, 10 mM, pH 7.4) containing 10 mM redox electrolyte $[Fe(CN)_6]^{3-/4-}$. A solution of $K_3Fe(CN)_6/K_4Fe(CN)_6$ (0.5 mM, 1:1, v/v) was used as the redox probe during the electrochemical studies using three electrode cells. All the experiments with AFM1 were carried out after taking proper care. After use, the residual solutions were inactivated by treating them with a mixture of 2.5% sodium hypochlorite and 0.25 N sodium hydroxide for 30 min.

2.2. Microwave-Assisted Synthesis of MoS_2 QDs. 0.5 g of sodium molybdate tetrahydrate and 0.25 g of L-cysteine were added into 50 mL of deionized water.[15] The mixture was stirred to dissolve the precursors and then transferred into a microwave vial (G-30 vial). The microwave-assisted synthesis was carried out at 20 W for 20 min, maintaining a pressure of 6.5 bar. After the reaction, the solution was allowed to cool down to room temperature (RT, 25 ± 2 °C). After centrifugation for 60 min at 7000 rpm, a light yellow supernatant containing MoS_2 QDs was obtained. For purification, the prepared QDs were treated with dichloromethane, followed by a filtration step using a 0.22 μm microporous membrane. The purified bright-yellow-colored QD solution was stored at 4 °C.

During the microwave-assisted synthesis, the crystal lattices generate unsaturated Mo atoms at the edge. At the same time, L-cysteine is oxidized to L-cystine (a disulfide dimer). They combine to form the MoS_2 product.

2.3. Synthesis of the MoS_2/UiO-66-NH_2 Composite. The UiO-66-NH_2 MOF was synthesized according to a previously reported solvothermal procedure with minor modifications.[16] 0.2 g of $ZrCl_4$ was dissolved (ultrasonication, 30 min) in 20 mL of a solvent mixture (HCl/DMF, 1:5, v/v). Similarly, 0.016 g of NH_2-BDC was dissolved in 20 mL of DMF. The above metal and ligand solutions were then mixed and left to react overnight in a Teflon-lined autoclave placed in a heated oven (80 °C). The formed product was collected and washed with DMF and ethanol, followed by vacuum drying for 12 h (80 °C). The formation of the MoS_2/UiO-66-NH_2 composite was also processed as per the above method, with an additional step of addition of 20 μL of MoS_2 QDs in the metal ion solution before mixing it with the ligand solution and starting the solvothermal reaction.

2.4. Preparation of the Antibody/MoS_2/UiO-66-NH_2 Sensor. 1 mg of the MoS_2/UiO-66-NH_2 sample was dispersed in 1 mL of deionized water through ultrasonication for 15 min. 10 μL of the prepared suspension was then drop-cast on the working area of the SPCE. The modified electrode was then left to dry at 80 °C in a vacuum oven. Next, 10 μL of the antibody solution (1 μg/mL) and 20 μL of a mixture of ethylcarbodiimide hydrochloride (EDC)/*N*-hydroxysuccinimide (NHS) (0.05 M each) in 0.1 M MES buffer were introduced onto the modified screen-printed electrode (SPE) and left to incubate for 2 h. The nonspecific binding sites were then blocked by the standard bovine serum albumin treatment method. Finally, the prepared biosensor was washed with PBS buffer and stored under refrigerated conditions (4 °C). Several batches of the antibody (Ab)/MoS_2/UiO-66-NH_2 bioelectrodes were prepared using the above method and employed for the quantification of the AFM1 analyte.

For quantification of AFM1, 10 μL of the sample analyte was introduced onto the sensor surface, and the antigen−antibody interaction was allowed to take place for 10 min, unless specified. The sensor was then washed with PBS buffer and investigated for its electrochemical response. All the different experiments have been performed in triplicate at pH 7 at RT, and the average values are reported.

2.5. Analysis of Spiked Milk Samples. Some milk samples were spiked with known concentrations (i.e., 0.2, 0.5, 1, 2, 5, and 10 ng mL^{-1}) of AFM1. The spiked samples were centrifuged for 20 min to remove their fat content before

https://doi.org/10.1021/acsomega.2c00126
ACS Omega 2022, 7, 17600−17608

analysis. The collected supernatant was analyzed with the Ab/MoS_2/UiO-66-NH_2 sensors. The validation for the sensor's performance for AFM1 was confirmed by HPLC (Waters) with a UV−vis detector at 362 nm.

3. RESULTS AND DISCUSSION

3.1. Morphological and Structural Studies. The morphological investigations of the UiO-66-NH_2- and MoS_2/UiO-66-NH_2-modified SPEs have been made using electron microscopies, as shown in Figure 1. The scanning electron microscopy (SEM) image of the UiO-66-NH_2/SPEs shows the coverage of the glassy carbon electrode (GCE) with MOF crystal with a size of around 250−300 nm (Figure 1A). Such a morphology of the synthesized MOF agrees well with the literature report.[17] The SEM image of the MoS_2/UiO-66-NH_2 composite over the SPEs is shown in Figure 1B. The particle size of the composite has become slightly larger than that of the MOF alone, and the particles are also relatively more homogeneous in shape. The structural analysis of the MoS_2 QDs and MoS_2/UiO-66-NH_2 composite is done with transmission electron microscopy (TEM) imaging (Figure 1C). The synthesized MoS_2 QDs are spherically sized with a diameter of around 6−8 nm. The TEM image of the MoS_2/UiO-66-NH_2 composite does not reveal the presence of QDs on the surface. It can be assumed that the QDs were entrapped within the MOF particles. The same has been confirmed by the energy-dispersive X-ray spectrometry-based elemental analysis. This analysis confirms the presence of both Zr (from UiO-66-NH_2) and Mo (from MoS_2 QDs) along with carbon, oxygen, and nitrogen contents (Figure 2).

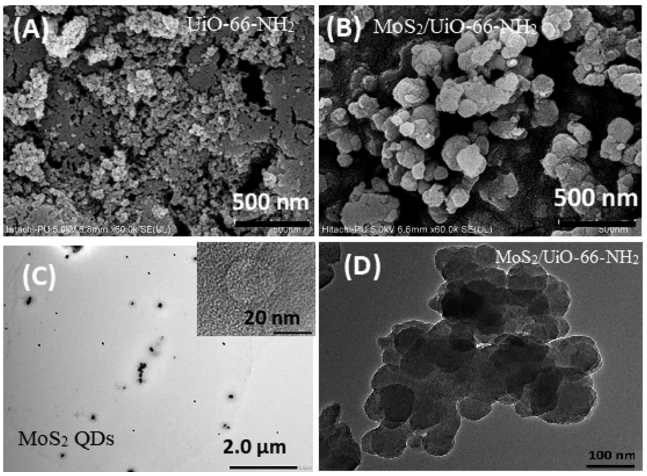

Figure 1. (A,B) SEM images of UiO-66-NH_2 and MoS_2/UiO-66-NH_2 composites deposited over the SPE, respectively; (C,D) TEM images of MoS_2 QDs and MoS_2/UiO-66-NH_2, respectively.

The X-ray diffraction (XRD) study (scan rate of 10 s/step) has been used to confirm the crystalline nature of the synthesized MoS_2/UiO-66-NH_2 nanocomposite (Figure 3A). In UiO-66-NH_2, the highest intensity peak (111) has been observed at 7.5°. The other characteristic peaks observed at 14.5° (002), 25.2° (600), and 32.7° (444) are also in agreement with the reported peaks of UiO-66-NH_2.[18] There is no compromise on the product crystallinity even when QDs are entrapped in the MOF matrix. As such, the XRD pattern of the nanocomposite shows much resolved and higher intensity peaks.

Figure 3B shows FTIR spectra of MoS_2 QDs, UiO-66-NH_2, and MoS_2/UiO-66-NH_2. In the MoS_2 QD sample, the bands at 3638, 1650, and 493 cm^{-1} correspond to the O−H stretching, N−H bending, and stretching frequency of Mo−S groups, respectively.[19] For MoS_2/UiO-66-NH_2, the appearance of bands at 3495/1579 and 1440/1278 cm^{-1} is assigned to the N−H stretching and C−N stretching frequencies, respectively, pertaining to the copresence of UiO-66-NH_2.[20]

The samples of MoS_2 QDs, UiO-66-NH_2, and MoS_2/UiO-66-NH_2 were also studied using their UV−vis absorption spectra (Figure 3C). In the MoS_2 QD sample, the shoulder peaks around 300 and 268 nm are assigned to the excitonic features and optical transitions.[21] The UV−vis spectrum of UiO-66-NH_2 shows two absorption peaks at 280 and 390 nm. The nanocomposite sample shows peaks related to both the QDs and UiO-66-NH_2 components, which indicate its successful formation. The composite shows an absorption peak at 273 nm and a broad absorption signal at 370 nm. The former peak (273 nm) is attributed to the ligand-to-metal charge transfer transitions, while the latter peak at 360 nm corresponds to interaction of the π^* orbital of the benzene ring with the lone pair on the nitrogen atom of amino groups.[22]

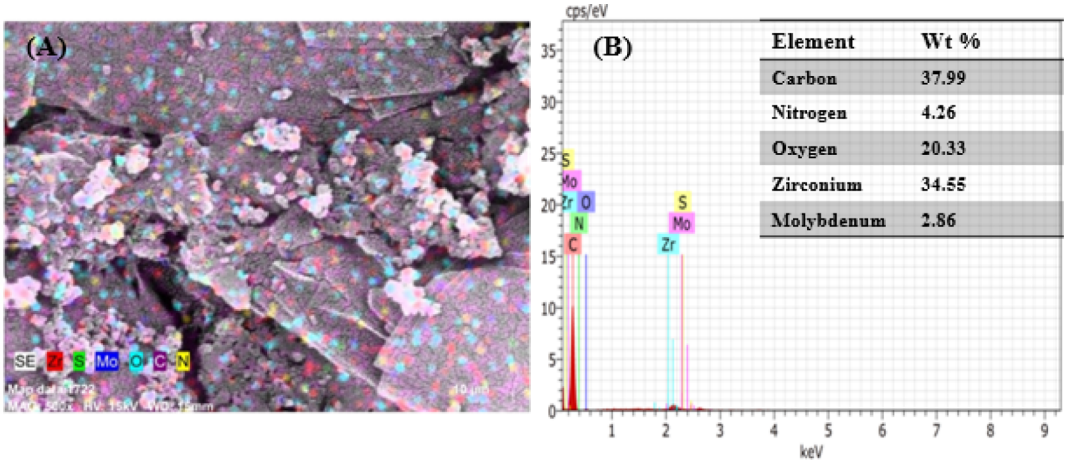

Figure 2. (A) Elemental mapping of different metals in MoS_2/UiO-66-NH_2, shown in different colors; (B) relative percentage distribution of different metals in MoS_2/UiO-66-NH_2.

https://doi.org/10.1021/acsomega.2c00126
ACS Omega 2022, 7, 17600−17608

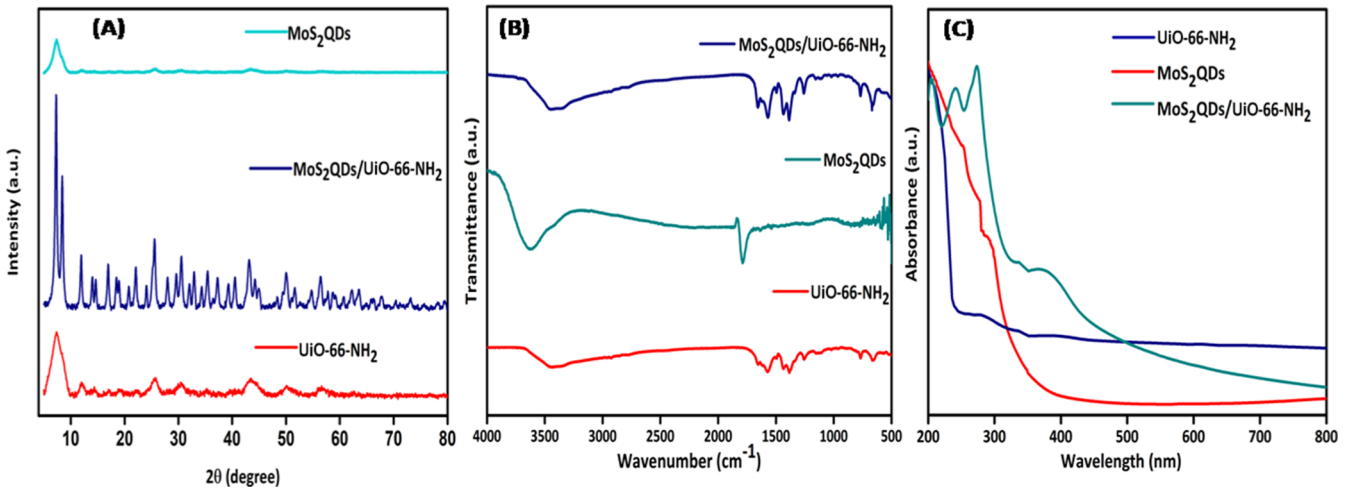

Figure 3. Characterizations of MoS_2 QDs, UiO-66-NH_2, and MoS_2/UiO-66-NH_2. (A) XRD patterns; (B) FTIR spectra; and (C) UV−vis absorption spectra.

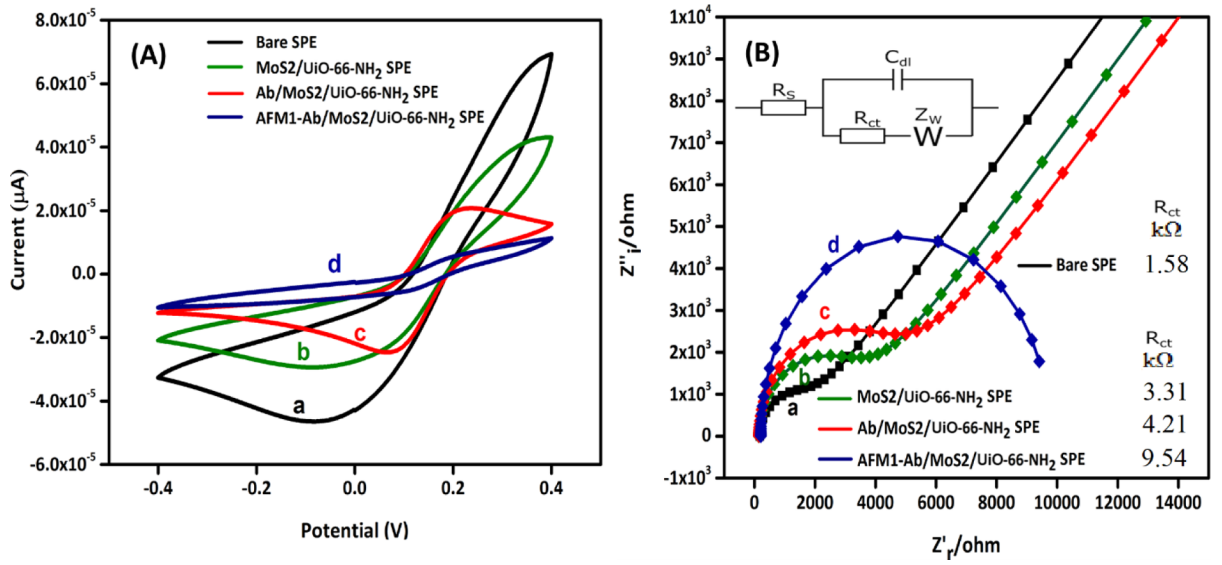

Figure 4. Electrochemical characterization of electrodes during different stages of sensor development. (A) Cyclic voltammograms and (B) EIS responses of the bare SPE, UiO-66-NH_2/MoS_2/SPE, Ab/MoS_2/UiO-66-NH_2/SPE, and AFM1/Ab/MoS_2/UiO-66-NH_2/SPE in a 10 mM, pH 7.4 PB saline medium containing 10 mM redox electrolyte $[Fe(CN)_6]^{3-/4-}$.

3.2. Electrochemical Studies and the Detection of AFM1 Using Ab/MoS_2/UiO-66-NH_2. *3.2.1. Cyclic Voltammetry Studies.* The electrochemical experiments were carried out with a three-electrode system wherein Ag/AgCl, the Pt wire, and SPEs were taken as reference, auxiliary, and working electrodes, respectively. The electrochemical impedance spectroscopy (EIS) experiments were performed in the frequency range of 0.1×10^5 Hz with a perturbation potential of 5 mV.

The Ab/MoS_2/UiO-66-NH_2 immunosensor electrodes were characterized by cyclic voltammetry (CV) measurements. Figure 4A shows the CV curves of the electrode during different stages of its preparation. The well-defined oxidation and reduction peaks are observed for the bare SPE owing to the electron transfer between the electrode and electrolyte solution. The intensity (extent of current values) decreases to some extent after the modification of the SPCE with the MoS_2/UiO-66-NH_2 composite. The immobilization of antibodies on the surface caused a further decrease in the redox peak current values, which is expected as the protein layer acts as a barrier for the surface charge transfer and also restricts the diffusion of the redox couple in the bulk electrode. A change in the peak-to-peak separation between the cathodic and anodic signals is another indicator of the fact that the electron-transfer kinetics is influenced. The introduction of the counter analyte, that is, AFM1, also results in a further decrease in the peak currents as the antigen−antibody (Ab-AFM1) complex forms and reduces the conductivity of the electrode surface. The CV studies have provided useful confirmation on the successful step-by-step modification of the SPE.

3.2.2. EIS-Based Bioassay Development for AFM1. EIS is an extremely useful electrochemical technique for the development of sensitive biosensors. EIS characteristics of the electrodes are recorded in the form of Nyquist plots. Nyquist plots recorded during the different stages of the sensor development are shown in Figure 4B. For the bare SPE, the value of R_{ct} is estimated to be 1.58 kΩ, which increases to 3.31 kΩ after its modification with the UiO-66-NH_2/MoS_2 composite. The attachment of antibodies further increases

https://doi.org/10.1021/acsomega.2c00126
ACS Omega 2022, 7, 17600−17608

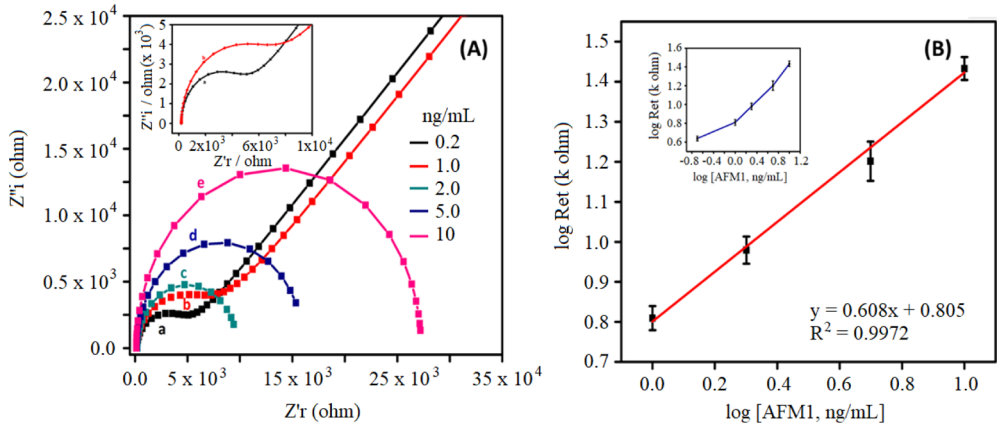

Figure 5. Bioassay of AFM1 with the Ab/MoS_2/UiO-66-NH_2/SPE biosensor. (A) EIS responses against different analyte concentrations and the (B) corresponding calibration plot. The electrolyte used was 10 mM, pH 7.4 PB saline solution containing 10 mM redox electrolyte $[Fe(CN)_6]^{3-/4-}$.

Table 1. Comparison of the Ab/MoS_2/UiO-66-NH_2/SPE Biosensor with Some Recently Reported Similar Electrochemical Sensors for AFM1

transducer platform	biorecognition element	method	detection range	LOD	refs
poly(neutral red) and carboxylated pillar [5] arene	aptamer	impedimetric (EIS)	5−120 ng L^{-1}	0.5 ng L^{-1}	23
SPE system	antibody	amperometric	30−160 pg mL^{-1}	25 pg mL^{-1}	24
gold-labeled anti-AFM1 combined with electrodeposition of Ag onto colloidal gold	aptamer	EIS	15−1000 and 25−125 ng mL^{-1}	15.0 and 25 ng mL^{-1}	25
label-free silver wire	antibody	EIS	6.25−100 pg mL^{-1}	1 pg mL^{-1}	26
aptamer-modified SPCEs	aptamer	EIS	2−150 ng L^{-1}	1.15 ng L^{-1}	27
Au nanoparticles	aptamer	differential pulse voltammetry (DPV)	2−600 ng L^{-1}	0.9 ng L^{-1}	28
silicon nanoparticles	aptamer	EIS	10−500 fM	4.53 fM	29
gold microelectrode array immunochip	antibody	EIS		8 ng mL^{-1}	30
Fe_3O_4/polyaniline-basedelectrochemical aptasensor	aptamer	CV and square wave voltammetry	6−60 ng L^{-1}	1.98 ng L^{-1}	6b
GO-CS/CeO_2-CSnanocomposite	antibody	DPV	0.01−1 μg L^{-1}	0.009 μg L^{-1}	31
MoS_2 QDs@UiO-66-NH_2 composite	antibody	CV and EIS	0.2−10 ng mL^{-1}	0.06 ng mL^{-1}	this work

the R_{ct} value to 4.21 kΩ, which is attributed to the formation of a less conducting protein layer. Once the Ab/MoS_2/UiO-66-NH_2/SPE is used for the analysis of AFM1, R_{ct} of the system increases again (e.g., 9.54 kΩ for 2 ng mL^{-1} AFM1) because of the formation of the antigen−antibody complex over the surface of the electrode. The antigen−antibody complex acts as a kinetic barrier for the charge transfer and hence results in an increase in the R_{ct} values directly in proportion to the concentration of the antigen being analyzed. As such, the EIS results are also in accordance with the CV results.

The detection of AFM1 (0.2, 1, 2, 5, and 10 ng mL^{-1}) with the Ab/MoS_2/UiO-66-NH_2/SPE biosensor has been investigated in detail by the EIS technique. Nyquist plots obtained for these studies are shown in Figure 5A. The values of R_{ct} have shown a regular increment as the concentration of AFM1 was increased from 0.2 to 10 ng mL^{-1}. The highest concentration of AFM1 (10 ng mL^{-1}) is characterized with a R_{ct} value of 27.1 kΩ. The calibration curve, depicting the dependence of R_{ct} values as a function of AFM1 concentration, is shown in Figure 5B. Under the experimental conditions for the development of the Ab/MoS_2/UiO-66-NH_2/SPE biosensor, the present system delivers an excellent linear profile (R^2 = 0.99) for a concentration range of 1−10 ng mL^{-1} AFM1. The detection limit of the biosensor is estimated as 0.06 ng mL^{-1} (LOD = 3 σ/m, where σ = standard deviation of the blank sample and m = slope of the curve). The limit of quantification (LOQ) has also been calculated by the formula "LOQ = 10 (σ/m)" and found to be 0.49 ng mL^{-1}.

A comparison of the performance of the Ab/MoS_2/UiO-66-NH_2/SPE biosensor with other recently reported similar electrochemical sensors is summarized in Table 1. Clearly, the Ab/MoS_2/UiO-66-NH_2/SPE biosensor has exhibited excellent performance in terms of the LOD. Its design is also simple, which can be easily translated into a cost-effective disposable option.

3.2.3. Selectivity of the Immunosensor. The selectivity of the Ab/MoS_2/UiO-66-NH_2/SPE biosensor has been tested against some common food contaminants, such as toxins (zearalenone), pesticides (atrazine, methyl parathion), a heavy metal (Pb^{2+}), and bacteria (*Escherichia coli*). The experimental conditions were kept identical in all these selectivity studies. As shown in Figure 6, the biosensor did not exhibit any significant R_{ct} response against the nonspecific analytes, and the signal was close to the baseline (blank) reading. A response (change in the R_{ct} value) was observed only for the AFM1 analyte. These studies clearly show the selective response of the Ab/MoS_2/UiO-66-NH_2/SPE biosensor toward AFM1.

3.2.4. Application of the Ab/MoS_2/UiO-66-NH_2/SPE Biosensor for the Detection of AFM1 in Spiked Milk Samples. The quantification of AFM1 in the spiked milk

https://doi.org/10.1021/acsomega.2c00126
ACS Omega 2022, 7, 17600−17608

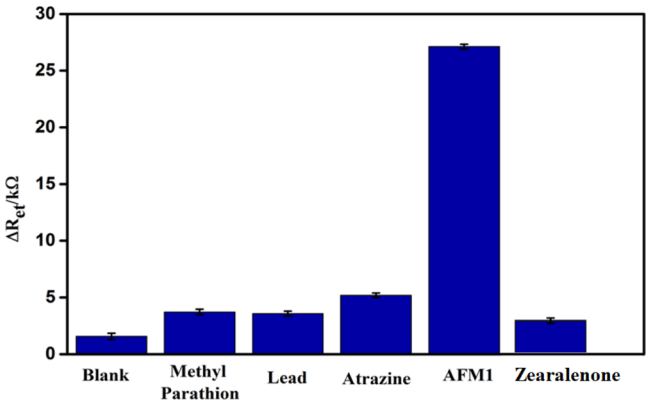

Figure 6. Response of the Ab/MoS_2/UiO-66-NH_2/SPE biosensor toward AFM1 and some other selected possibly interfering analytes. Concentration of analytes = 10 ng mL^{-1} in 10 mM, pH 7.4 PB saline solution containing 10 mM redox electrolyte $[Fe(CN)_6]^{3-/4-}$.

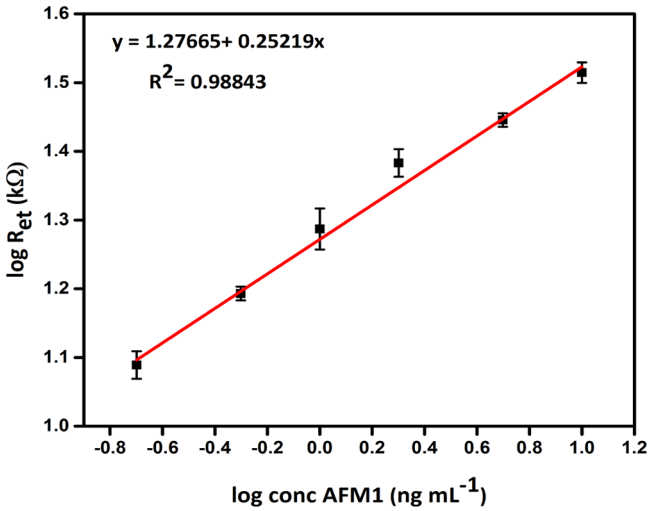

Figure 8. Analysis of different spiked milk samples (0.2, 0.5, 1, 2, 5, 10 ng mL^{-1}) with the Ab/MoS_2/UiO-66-NH_2/SPE biosensor. Electrolyte = 10 mM, pH 7.4 PB saline solution containing 10 mM redox electrolyte $[Fe(CN)_6]^{3-/4-}$.

samples was established by the HPLC technique.[32] For this, 10 mL of the spiked milk sample was diluted with 100 mL of ultrapure water and then filtered through a 0.45 μm filter paper. It was then centrifuged at 8000 rpm for 20 min to separate out the fat before introducing the sample (aliquots of 10 μL) into the HPLC column. The analysis was performed using a C18 column (Thermo Fisher 120, 50 mm × 2.1 mm × 5 μm). An eluent mixture of acetonitrile: water (35:65) was used as the mobile phase gradient. The flow rate during the analysis was maintained to 1 mL min^{-1}. For detection, the signal from the UV−vis detector at 362 nm wavelength was measured. The collected chromatograms are shown in Figure 7. The retention time of AFM1 was at 1.39 min, and the blank sample did not show any interference. The HPLC-verified samples were then tested with the Ab/MoS_2/UiO-66-NH_2/SPE biosensor.

The Ab/MoS_2/UiO-66-NH_2/SPE biosensor was used to detect AFM1 in spiked milk samples to verify its practical utility. The aliquots, collected after the centrifugation of the spiked milk samples, were introduced over the working area of the sensor and left to incubate for 5 min. The electrode was then gently washed with water and studied for its EIS characteristics using the $[Fe(CN)_6]^{3-/4-}$ redox probe. The recorded values of R_{ct} were converted into the concentration values using the calibration curves, as shown in Figure 8 (y = 1.28 + 0.252x). The R_{ct} values from this study match well with the data collected with the standard buffer solutions. Therefore, the Ab/MoS_2/UiO-66-NH_2/SPE biosensor for AFM1 has a clear potential to be used for practical applications. The concentrations of the AFM1 analyte in the spiked milk samples were also validated with a reference HPLC method. The HPLC-based data also corroborated the excellent performance of the Ab/MoS_2/UiO-66-NH_2/SPE biosensor toward the detection of AFM1.

In recent years, the utility of QDs, for example, graphene and MoS_2 nanosheets, for the development of electrochemical biosensors has been well recognized. These nanomaterials facilitate better electrocatalytic activities and high surface areas. The integration of MoS_2 QDs with MOFs provides multiple advantages as far as the biosensor preparation is concerned. First, the MoS_2/UiO-66-NH_2 composite ensures a high surface area to the transducer material which is important to achieve an efficient immobilization of the antibodies. Furthermore, UiO-66-NH_2 brings the readily available −NH_2 functionality which minimizes the application of chemical treatment to the transducer material. In addition to this, the presence of a

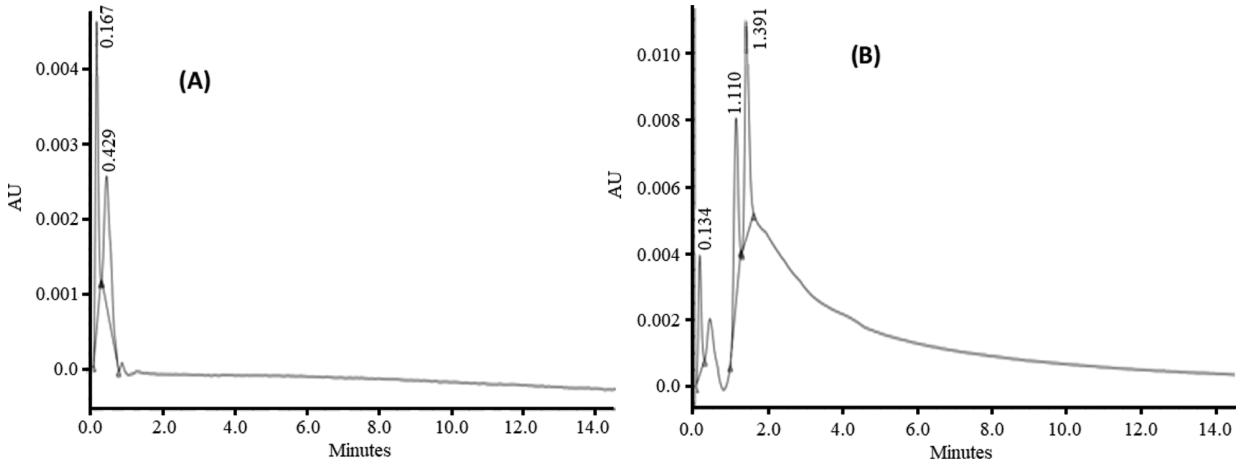

Figure 7. HPLC chromatograms of the (A) blank milk sample and (B) milk sample spiked with AFM1.

https://doi.org/10.1021/acsomega.2c00126
ACS Omega 2022, 7, 17600−17608

porous MOF allows the diffusion of the analyte within the sensor surface. This leads to a better signal stability and sensor reproducibility.

4. CONCLUSIONS

In the present study, the MoS_2 QDs have been incorporated within a UiO-66-NH_2 matrix to prepare a novel functional composite. MoS_2 QDs have a high theoretical capacity, a good electrochemical activity, and a superior chemical stability. MOFs, as such, do not possess enough electrochemical activity due to the presence of coordinate bonding between the metal and the linker. The SPEs of MOFs exhibit a high resistivity and consequently also exhibit a high value of charge transfer resistance. The MoS_2/UiO-66-NH_2 composite has the necessary electrochemical activity, high surface area, and amine functionality which advocate its application for the development of electrochemical biosensors. The antibody-conjugated MoS_2/UiO-66-NH_2 has been used to prepare an SPE biosensor for the detection of AFM1 using CV and EIS. The analytical performance of the biosensor is established in terms of its high sensitivity, low LOD (0.06 ng mL^{-1}), wide detection range (0.2−10 ng mL^{-1}), and specificity. In addition, the practicality of the sensor is further established by analyzing the detection of AFM1 in some spiked milk samples. This approach can also be extended for the detection of other AFs such as AFB1.

AUTHOR INFORMATION

Corresponding Author

Akash Deep − *Academy of Scientific and Innovative Research (AcSIR), Ghaziabad 201002 Uttar Pradesh, India; CSIR-Central Scientific Instruments Organization (CSIR-CSIO), Chandigarh 160030, India;* orcid.org/0000-0002-6382-6104; Phone: +91-172-2672236; Email: dr.akashdeep@csio.res.in

Authors

Gurjeet Kaur − *Academy of Scientific and Innovative Research (AcSIR), Ghaziabad 201002 Uttar Pradesh, India; CSIR-Central Scientific Instruments Organization (CSIR-CSIO), Chandigarh 160030, India*

Saloni Sharma − *Academy of Scientific and Innovative Research (AcSIR), Ghaziabad 201002 Uttar Pradesh, India; CSIR-Central Scientific Instruments Organization (CSIR-CSIO), Chandigarh 160030, India*

Shalini Singh − *Academy of Scientific and Innovative Research (AcSIR), Ghaziabad 201002 Uttar Pradesh, India; CSIR-Central Scientific Instruments Organization (CSIR-CSIO), Chandigarh 160030, India*

Neha Bhardwaj − *Department of Biotechnology, University Institute of Engineering Technology (UIET), Panjab University, Chandigarh 160014, India;* orcid.org/0000-0002-1566-0445

Complete contact information is available at: https://pubs.acs.org/10.1021/acsomega.2c00126

Notes

The authors declare no competing financial interest.

ACKNOWLEDGMENTS

Authors are thankful to the director CSIR-CSIO, Chandigarh, for all the facilities. The financial assistance from SERB, India, through project no. EMR/2016/006480 is gratefully acknowledged.

REFERENCES

(1) (a) Rushing, B. R.; Selim, M. I. Aflatoxin B1: A review on metabolism, toxicity, occurrence in food, occupational exposure, and detoxification methods. *Food Chem. Toxicol.* **2019**, *124*, 81−100. (b) Kumar, P.; Mahato, D. K.; Kamle, M.; Mohanta, T. K.; Kang, S. G. Aflatoxins: a global concern for food safety, human health and their management. *Front. Microbiol.* **2017**, *07*, 2170. (c) Benkerroum, N. Chronic and acute toxicities of aflatoxins: mechanisms of action. *Int. J. Environ. Res. Public Health* **2020**, *17*, 423. (d) Ferreira, R. G.; Cardoso, M. V.; de Souza Furtado, K. M.; Espíndola, K. M. M.; Amorim, R. P.; Monteiro, M. C. Epigenetic alterations caused by aflatoxin b1: a public health risk in the induction of hepatocellular carcinoma. *Transl. Res.* **2019**, *204*, 51−71.

(2) (a) Nguyen, T.; Flint, S.; Palmer, J. Control of aflatoxin M1 in milk by novel methods: A review. *Food Chem.* **2020**, *311*, 125984. (b) Flores-Flores, M. E.; Lizarraga, E.; López de Cerain, A.; González-Peñas, E. Presence of mycotoxins in animal milk: A review. *Food Control* **2015**, *53*, 163−176. (c) Min, L.; Li, D.; Tong, X.; Sun, H.; Chen, W.; Wang, G.; Zheng, N.; Wang, J. The challenges of global occurrence of aflatoxin M1 contamination and the reduction of aflatoxin M1 in milk over the past decade. *Food Control* **2020**, *117*, 107352.

(3) (a) Afum, C.; Cudjoe, L.; Hills, J.; Hunt, R.; Padilla, L.; Elmore, S.; Afriyie, A.; Opare-Sem, O.; Phillips, T.; Jolly, P. Association between aflatoxin M1 and liver disease in HBV/HCV infected persons in Ghana. *Int. J. Environ. Res. Public Health* **2016**, *13*, 377. (b) Giovati, L.; Magliani, W.; Ciociola, T.; Santinoli, C.; Conti, S.; Polonelli, L. AFM1 in milk: physical, biological, and prophylactic methods to mitigate contamination. *Toxins* **2015**, *7*, 4330−4349. (c) Marchese, S.; Polo, A.; Ariano, A.; Velotto, S.; Costantini, S.; Severino, L. Aflatoxin B1 and M1: Biological properties and their involvement in cancer development. *Toxins* **2018**, *10*, 214.

(4) Omar, S. S. Aflatoxin M1 levels in raw milk, pasteurised milk and infant formula. *Ital. J. Food Saf.* **2016**, *5*, 5788.

(5) (a) Busman, M.; Bobell, J. R.; Maragos, C. M. Determination of the aflatoxin M1 (AFM1) from milk by direct analysis in real time−mass spectrometry (DART-MS). *Food Control* **2015**, *47*, 592−598. (b) Mao, J.; Lei, S.; Liu, Y.; Xiao, D.; Fu, C.; Zhong, L.; Ouyang, H. Quantification of aflatoxin M1 in raw milk by a core-shell column on a conventional HPLC with large volume injection and step gradient elution. *Food Control* **2015**, *51*, 156−162. (c) Cavaliere, C.; Foglia, P.; Pastorini, E.; Samperi, R.; Laganà, A. Liquid chromato-graphy/tandem mass spectrometric confirmatory method for determining aflatoxin M1 in cow milk comparison between electrospray and atmospheric pressure photoionization sources. *J. Chromatogr.* **2006**, *1101*, 69−78. (d) Khodadadi, M.; Malekpour, A.; Mehrgardi, M. A. Aptamer functionalized magnetic nanoparticles for effective extraction of ultratrace amounts of aflatoxin M1 prior its determination by HPLC. *J. Chromatogr. A* **2018**, *1564*, 85−93. (e) Lin, L.; Zhang, J.; Wang, P.; Wang, Y.; Chen, J. Thin-layer chromatography of mycotoxins and comparison with other chromatographic methods. *J. Chromatogr. A* **1998**, *815*, 3−20.

(6) (a) Pang, Y.-H.; Guo, L.-L.; Shen, X.-F.; Yang, N.-C.; Yang, C. Rolling circle amplified DNAzyme followed with covalent organic frameworks: Cascade signal amplification of electrochemical ELISA for alfatoxin M1 sensing. *Electrochim. Acta* **2020**, *341*, 136055. (b) Nguyen, B. H.; Tran, L. D.; Do, Q. P.; Nguyen, H. L.; Tran, N. H.; Nguyen, P. X. Label-free detection of aflatoxin M1 with electrochemical Fe3O4/polyaniline-based aptasensor. *Mater. Sci. Eng., C* **2013**, *33*, 2229−2234. (c) Tarannum, N.; Nipa, M. N.; Das, S.; Parveen, S. Aflatoxin M1 detection by ELISA in raw and processed milk in Bangladesh. *Toxicol. Rep.* **2020**, *7*, 1339−1343.

(7) (a) Singh, H.; Bamrah, A.; Bhardwaj, S. K.; Deep, A.; Khatri, M.; Kim, K.-H.; Bhardwaj, N. Nanomaterial-based fluorescent sensors for the detection of lead ions. *J. Hazard. Mater.* **2021**, *407*, 124379. (b) Chen, H.; Zhang, L.; Hu, Y.; Zhou, C.; Lan, W.; Fu, H.; She, Y.

Nanomaterials as optical sensors for application in rapid detection of food contaminants, quality and authenticity. *Sens. Actuators, B* **2020**, *329*, 129135. (c) Wang, W.; Wang, X.; Cheng, N.; Luo, Y.; Lin, Y.; Xu, W.; Du, D. Recent advances in nanomaterials-based electrochemical (bio) sensors for pesticides detection. *Trends Anal. Chem.* **2020**, *132*, 116041.

(8) (a) Xue, Z.; Zhang, Y.; Yu, W.; Zhang, J.; Wang, J.; Wan, F.; Kim, Y.; Liu, Y.; Kou, X. Recent advances in aflatoxin B1 detection based on nanotechnology and nanomaterials-A review. *Anal. Chim. Acta* **2019**, *1069*, 1−27. (b) Danesh, N. M.; Bostan, H. B.; Abnous, K.; Ramezani, M.; Youssefi, K.; Taghdisi, S. M.; Karimi, G. Ultrasensitive detection of aflatoxin B1 and its major metabolite aflatoxin M1 using aptasensors: A review. *Trends Anal. Chem.* **2018**, *99*, 117−128. (c) Eivazzadeh-Keihan, R.; Pashazadeh, P.; Hejazi, M.; de la Guardia, M.; Mokhtarzadeh, A. Recent advances in nanomaterial-mediated bio and immune sensors for detection of aflatoxin in food products. *Trends Anal. Chem.* **2017**, *87*, 112−128. (d) Liu, D.; Li, W.; Zhu, C.; Li, Y.; Shen, X.; Li, L.; Yan, X.; You, T. Recent progress on electrochemical biosensing of aflatoxins: A review. *Trends Anal. Chem.* **2020**, *133*, 115966.

(9) (a) Bhardwaj, H.; Singh, C.; Pandey, M. K.; Sumana, G. Star shaped zinc sulphide quantum dots self-assembled monolayers: Preparation and applications in food toxin detection. *Sens. Actuators, B* **2016**, *231*, 624−633. (b) Gu, C.; Yang, L.; Wang, M.; Zhou, N.; He, L.; Zhang, Z.; Du, M. A bimetallic (Cu-Co) Prussian Blue analogue loaded with gold nanoparticles for impedimetric aptasensing of ochratoxin a. *Microchim. Acta* **2019**, *186*, 343. (c) Wang, Z.; Yu, H.; Han, J.; Xie, G.; Chen, S. Rare Co/Fe-MOFs exhibiting high catalytic activity in electrochemical aptasensors for ultrasensitive detection of ochratoxin A. *Chem. Commun.* **2017**, *53*, 9926−9929.

(10) (a) Bolotsky, A.; Butler, D.; Dong, C.; Gerace, K.; Glavin, N. R.; Muratore, C.; Robinson, J. A.; Ebrahimi, A. Two-dimensional materials in biosensing and healthcare: from in vitro diagnostics to optogenetics and beyond. *ACS Nano* **2019**, *13*, 9781−9810. (b) Sebastian, A.; Zhang, F.; Dodda, A.; May-Rawding, D.; Liu, H.; Zhang, T.; Terrones, M.; Das, S. Electrochemical polishing of two-dimensional materials. *ACS Nano* **2018**, *13*, 78−86. (c) Mathew, M.; Radhakrishnan, S.; Vaidyanathan, A.; Chakraborty, B.; Rout, C. S. Flexible and wearable electrochemical biosensors based on two-dimensional materials: Recent developments. *Anal. Bioanal. Chem.* **2021**, *413*, 727−762. (d) Wang, J. J.; Liu, Y.; Ding, Z.; Zhang, L.; Han, C.; Yan, C.; Amador, E.; Yuan, L.; Wu, Y.; Song, C. The exploration of quantum dot-molecular beacon based MoS2 fluorescence probing for myeloma-related Mirnas detection. *Bioact. Mater.* **2022**, *17*, 360−368.

(11) (a) Kukkar, M.; Sharma, A.; Kumar, P.; Kim, K.-H.; Deep, A. Application of MoS2 modified screen-printed electrodes for highly sensitive detection of bovine serum albumin. *Anal. Chim. Acta* **2016**, *939*, 101−107. (b) Dalila R, N.; Md Arshad, M. K.; Gopinath, S. C. B.; Norhaimi, W. M. W.; Fathil, M. F. M. Current and future envision on developing biosensors aided by 2D molybdenum disulfide (MoS2) productions. *Biosens. Bioelectron.* **2019**, *132*, 248−264. (c) Yuan, Y.; Guo, R.-t.; Hong, L.-f.; Ji, X.-y.; Li, Z.-s.; Lin, Z.-d.; Pan, W.-g. Recent advances and perspectives of MoS2-based materials for photocatalytic dyes degradation: A review. *Colloids Surf., A* **2021**, *611*, 125836.

(12) Kukkar, M.; Singh, S.; Kumar, N.; Tuteja, S. K.; Kim, K.-H.; Deep, A. Molybdenum disulfide quantum dot based highly sensitive impedimetric immunoassay for prostate specific antigen. *Microchim. Acta* **2017**, *184*, 4647−4654.

(13) (a) Liu, S.; Lai, C.; Liu, X.; Li, B.; Zhang, C.; Qin, L.; Huang, D.; Yi, H.; Zhang, M.; Li, L.; Wang, W.; Zhou, X.; Chen, L. Metal-organic frameworks and their derivatives as signal amplification elements for electrochemical sensing. *Coord. Chem. Rev.* **2020**, *424*, 213520. (b) Rani, S.; Sharma, B.; Malhotra, R.; Kumar, S.; Varma, R. S.; Dilbaghi, N. Sn-MOF@ CNT nanocomposite: An efficient electrochemical sensor for detection of hydrogen peroxide. *Environ. Res.* **2020**, *191*, 110005. (c) Bhardwaj, S. K.; Bhardwaj, N.; Kaur, R.; Mehta, J.; Sharma, A. L.; Kim, K.-H.; Deep, A. An overview of different strategies to introduce conductivity in metal−organic frameworks and miscellaneous applications thereof. *J. Mater. Chem. A* **2018**, *6*, 14992−15009. (d) Liu, X.; Zhang, L.; Wang, J. Design Strategies for MOF-derived Porous Functional Materials: Preserving Surfaces and Nurturing Pores. *J. Materiomics* **2021**, *7*, 440−459.

(14) (a) Asadpour, O.; Rahbarizadeh, F. Phospholipase-Cγ1 Signaling Protein Down-Regulation by Oligoclonal-VHHs based Immuno-Liposome: A Potent Metastasis Deterrent in HER2 Positive Breast Cancer Cells. *Cell Junctions* **2020**, *22*, 30. (b) Lu, L.; Hu, X.; Zhu, Z.; Li, D.; Tian, S.; Chen, Z. Electrochemical Sensors and Biosensors Modified with Binary Nanocomposite for Food Safety. *J. Electrochem. Soc.* **2019**, *167*, 037512.

(15) Chang, K.; Chen, W. L-Cysteine-Assisted Synthesis of Layered MoS2/Graphene Composites with Excellent Electrochemical Performances for Lithium Ion Batteries. *ACS Nano* **2011**, *5*, 4720−4728. (b) Yang, L.; Wang, S.; Mao, J.; Deng, J.; Gao, Q.; Tang, Y.; Schmidt, O. G. Hierarchical MoS2/Polyaniline Nanowires with Excellent Electrochemical Performance for Lithium-Ion Batteries. *Adv. Mater.* **2013**, *25*, 1180−1184.

(16) Katz, M. J.; Brown, Z. J.; Colón, Y. J.; Siu, P. W.; Scheidt, K. A.; Snurr, R. Q.; Hupp, J. T.; Farha, O. K. A facile synthesis of UiO-66, UiO-67 and their derivatives. *Chem. Commun.* **2013**, *49*, 9449−9451.

(17) Ling, P.; Lei, J.; Jia, L.; Ju, H. Platinum nanoparticles encapsulated metal−organic frameworks for the electrochemical detection of telomerase activity. *Chem. Commun.* **2016**, *52*, 1226−1229.

(18) Hao, X.; Jin, Z.; Yang, H.; Lu, G.; Bi, Y. Peculiar synergetic effect of MoS2 quantum dots and graphene on Metal-Organic Frameworks for photocatalytic hydrogen evolution. *Appl. Catal., B* **2017**, *210*, 45−56.

(19) Li, Y.; Wang, X.; Liu, M.; Luo, H.; Deng, L.; Huang, L.; Wei, S.; Zhou, C.; Xu, Y. Molybdenum Disulfide Quantum Dots Prepared by Bipolar-Electrode Electrochemical Scissoring. *Nanomaterials* **2019**, *9*, 906.

(20) Kandiah, M.; Nilsen, M. H.; Usseglio, S.; Jakobsen, S.; Olsbye, U.; Tilset, M.; Larabi, C.; Quadrelli, E. A.; Bonino, F.; Lillerud, K. P. Synthesis and stability of tagged UiO-66 Zr-MOFs. *Chem. Mater.* **2010**, *22*, 6632−6640.

(21) Zhou, K.; Zhang, Y.; Xia, Z.; Wei, W. As-prepared MoS2 quantum dot as a facile fluorescent probe for long-term tracing of live cells. *Nanotechnology* **2016**, *27*, 275101.

(22) Mehta, J.; Dhaka, S.; Paul, A. K.; Dayananda, S.; Deep, A. Organophosphate hydrolase conjugated UiO-66-NH2 MOF based highly sensitive optical detection of methyl parathion. *Environ. Res.* **2019**, *174*, 46−53.

(23) Smolko, V.; Shurpik, D.; Porfireva, A.; Evtugyn, G.; Stoikov, I.; Hianik, T. Electrochemical aptasensor based on poly (neutral red) and carboxylated pillar [5] arene for sensitive determination of aflatoxin M1. *Electroanalysis* **2018**, *30*, 486−496.

(24) Micheli, L.; Grecco, R.; Badea, M.; Moscone, D.; Palleschi, G. An electrochemical immunosensor for aflatoxin M1 determination in milk using screen-printed electrodes. *Biosens. Bioelectron.* **2005**, *21*, 588−596.

(25) Vig, A.; Radoi, A.; Muñoz-Berbel, X.; Gyemant, G.; Marty, J.-L. Impedimetric aflatoxin M1 immunosensor based on colloidal gold and silver electrodeposition. *Sens. Actuators, B* **2009**, *138*, 214−220.

(26) Bacher, G.; Pal, S.; Kanungo, L.; Bhand, S. A label-free silver wire based impedimetric immunosensor for detection of aflatoxin M1 in milk. *Sens. Actuators, B* **2012**, *168*, 223−230.

(27) Istamboulié, G.; Paniel, N.; Zara, L.; Granados, L. R.; Barthelmebs, L.; Noguer, T. Development of an impedimetric aptasensor for the determination of aflatoxin M1 in milk. *Talanta* **2016**, *146*, 464−469.

(28) Jalalian, S. H.; Ramezani, M.; Danesh, N. M.; Alibolandi, M.; Abnous, K.; Taghdisi, S. M. A novel electrochemical aptasensor for detection of aflatoxin M1 based on target-induced immobilization of gold nanoparticles on the surface of electrode. *Biosens. Bioelectron.* **2018**, *117*, 487−492.

https://doi.org/10.1021/acsomega.2c00126
ACS Omega 2022, 7, 17600−17608

(29) Ben Aissa, S.; Mars, A.; Catanante, G.; Marty, J.-L.; Raouafi, N. Design of a redox-active surface for ultrasensitive redox capacitive aptasensing of aflatoxin M1 in milk. *Talanta* **2019**, *195*, 525−532.
(30) Parker, C. O.; Lanyon, Y. H.; Manning, M.; Arrigan, D. W. M.; Tothill, I. E. Electrochemical immunochip sensor for aflatoxin M1 detection. *Anal. Chem.* **2009**, *81*, 5291−5298.
(31) An, X.; Shi, X.; Zhang, H.; Yao, Y.; Wang, G.; Yang, Q.; Xia, L.; Sun, X. An electrochemical immunosensor based on a combined amplification strategy with the GO−CS/CeO2−CS nanocomposite for the detection of aflatoxin M 1. *New J. Chem.* **2020**, *44*, 1362−1370.
(32) Mendonça, C.; Venâncio, A. Fate of aflatoxin M1 in cheese whey processing. *J. Sci. Food Agric.* **2005**, *85*, 2067−2070.

https://doi.org/10.1021/acsomega.2c00126
ACS Omega 2022, 7, 17600−17608